Microwave Filters With Improved Spurious Performance Based on Sandwiched Conductor Dielectric Resonators

Andrew R. Weily and Ananda S. Mohan

***Abstract*—Microwave filters based on a novel resonator comprised of a sandwiched conductor dielectric resonator (SCDR) loaded in a cylindrical cavity are analyzed in this paper. The SCDR is a compact resonator that exhibits good spurious performance. Resonant frequencies of the lower order modes are analyzed, and mode charts, unloaded Q, slot coupling, and screw coupling graphs are presented. S-parameters are computed using the finite-difference time-domain (FDTD) method for one- and four-pole SCDR filters and compared with measured results. The measured spurious performance for the four-pole elliptic function filter shows a large improvement over conventional dielectric-resonator filters. The measured results agree closely with predicted values obtained using the FDTD method.**

***Index Terms*—Dielectric-resonator filter, FDTD analysis, mode chart, sandwiched conductor dielectric resonator, spurious performance.**

I. Introduction

Mobile communication systems require filters that have good in-band performance in terms of loss and good out-of-band spurious performance. Filters composed of dielectric resonators (DRs) give excellent in-band performance, but have poor spurious characteristics due to their crowded mode spectrum. The key issue in obtaining wide spurious rejection performance from a filter is to optimally design the resonator to give a well-spaced mode spectrum. Charts have been presented by Kobayashi and Miura specifically for this purpose [1]. When using the TE_{01}-mode DR, introducing a concentric hole can markedly improve the spurious performance [1], [2]. Many other techniques have also been presented over the years to further improve the spurious performance of DR filters. Quarter-wavelength coaxial TM_{01}-mode DRs have been shown to have moderate insertion loss and good spurious performance [3]. Mode suppressors have been added to filters to suppress out-of-band spurious modes [4], and for TE_{01}-mode DR filters resonant evanescent-mode bandpass irises may be used to filter out undesired modes [5]. Rectangular DRs excited in the TM_{110}-mode [6] and cylindrical TM_{01}-mode DRs [7] have also been shown to produce filters with good separation between spurious passbands. Quarter-cut TE_{01}-mode DRs reported in [8] are able to suppress TM_{01} and hybrid modes with azimuthal variation index $n = 1$, as well as having low insertion loss.

The concept of using different waveguide cavities to improve stopband rejection was introduced over 30 years ago [9]. This concept has been applied to half-wave coaxial DRs [10], as well as hybrid dominant TM_{01}-mode dielectric rod resonators and regular TM_{01}-mode disk DRs [11] to produce filters with improved stopband performance. Another successful technique that has been presented for air-filled cylindrical cavities involves replacing the input cavities with lower order mode resonators that possess good spurious-mode separation [12]. This method achieves greater than 50-dB spurious suppression to just over twice the filter center frequency. Encouraged by these results, researchers began to design mixed-mode DR filters in both cylindrical [13] and rectangular [14] enclosures, combining TE_{01} and HE_{11} DR modes to achieve good out-of-band performance. Another successful approach mixes completely different resonators such as combline and TE_{01}-mode DRs [15], [16] or conductor and dielectric loaded resonators [17] to achieve extremely low-passband insertion losses and excellent spurious-mode suppression. Other notable systems are rectangular DR filters [18], partially metallized dielectric slugs [19], conductor loaded DRs [20], modified combline filters that mix stepped and uniform rods [21], dielectric combline filters [22], and conductor loaded filters [23].

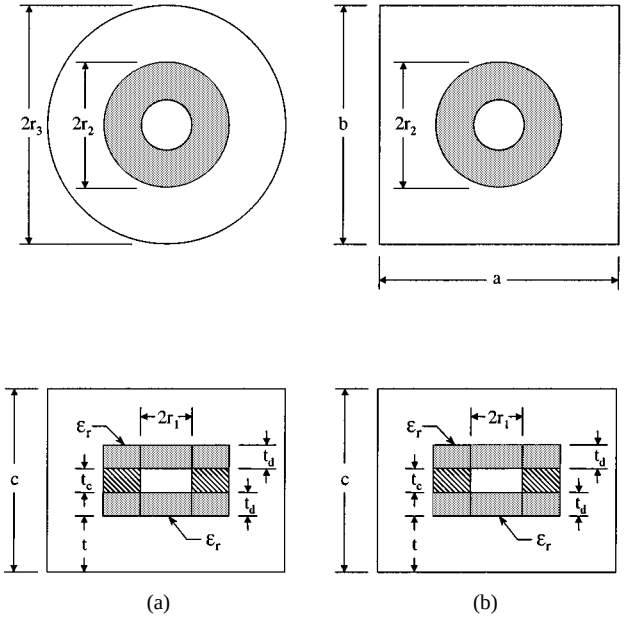

Fig. 1. (a) Configuration of an SCDR loaded in a cylindrical cavity. (b) Configuration of an SCDR loaded in a rectangular cavity.

Several researchers have reported novel filter elements that provide some improvement over conventional DR filters. Conductor loaded resonators were introduced to counter the spurious-free performance limitations of DR microwave filters [23], but have limited scope for miniaturization. In 1999, resonators composed of both dielectric and conductor materials were reported, such as the partially metallized dielectric cylinder [19] and the conductor-loaded DR [20]. These resonators are generally compact, have moderately high Q (lower than DRs), but offer limited improvements in spurious performance. Hence, with an aim to improve spurious performance of microwave filters, a novel compact resonator configuration is introduced in this paper, and its performance is investigated via theoretical calculations and measurement. The resonator, first proposed by the authors in 1998 [24], consists of a cylindrical conductor sandwiched between two DRs and is denoted as the sandwiched conductor dielectric resonator (SCDR). The SCDR can be made very compact and has moderately high Q, but offers considerable improvements in spurious performance.

In this paper, the new SCDR configuration is rigorously analyzed using finite-difference time-domain (FDTD) analysis methods [25]–[27]. To confirm the improved spurious rejection performance of the SCDR, resonant frequencies of the lower order modes are computed using both the FDTD method and HFSS and compared with measured results. Mode charts are calculated for the SCDR loaded in both cylindrical and rectangular cavities to clearly show the variation of the mode separation obtained by changing various parameters of the configuration. An unloaded Q chart and slot coupling graph are also calculated to aid in the design of the SCDR filter. To further verify the improved spurious performance, the S-parameters of a probe-coupled one-pole SCDR filter are obtained using modal extraction and the

Manuscript received September 13, 2000. This work was supported by the Australian Research Council under an Australian Postgraduate Research Award.

The authors are with the Faculty of Engineering, Telecom Group, University of Technology, Sydney, N.S.W. 2007, Australia (e-mail: ananda@eng.uts.edu.au).

Publisher Item Identifier S 0018-9480(01)06133-6.

TABLE I
DIMENSIONS, THEORETICAL RESONANT FREQUENCY, AND Q_u FOR TWO CONFIGURATIONS OF HE_{11}-MODE SCDR. REFER TO FIG. 1(a) FOR PARAMETER DEFINITIONS. ALL DIMENSIONS ARE IN MILLIMETERS

	ε_r	$2r_3$	$2r_2$	$2r_1$	c	t_c	t_d	t	f_0	Q_u
SCDR 1	37	71	46.2	25.4	62	1	2.5	28	1.977GHz	5,892
SCDR 2	45	40.9	26.6	14.6	35.7	0.5	7.2	10.4	1.900GHz	7,730

TABLE II
COMPARISON OF MEASURED RESONANT FREQUENCIES WITH THOSE CALCULATED USING THE FDTD METHOD FOR THE SCDR CAVITY OF FIG. 1(a), WITH THE DIMENSIONS GIVEN FOR SCDR 1 IN TABLE I

	HE_{11}	TM_{01}	HE_{21}	TM_{02}	HE_{12}
Measured	1.980	3.100	3.503	3.888	4.133
FDTD (Error)	1.977 (0.15%)	3.097 (0.10%)	3.465 (1.08%)	3.871 (0.44%)	4.146 (0.31%)
HFSS™	2.043	3.183	3.590	3.969	4.130
Relative Mode Spectrum	$1.0f_0$	$1.57f_0$	$1.77f_0$	$1.96f_0$	$2.09f_0$

TABLE III
VOLUME AND CAVITY UNLOADED Q FOR CONDUCTOR LOADED AND SCDR CAVITIES AT PCS FREQUENCIES

Cavity Type	Volume(cm^3)	Resonator Q_u	Q_u/Volume
Conductor Loaded [23]	250.4/2	6,000 (measured)	48
SCDR 1 (Table 1)	245.5/2	4,700 (measured)	38
SCDR 2 (Table 1)	46.9/2	7,730 (FDTD)	330

FDTD method and compared with measured results. Finally, a four-pole HE_{11}-mode elliptic-function SCDR filter prototype is designed and built and its measured performance recorded. The four-pole filter is simulated using the FDTD method and compared with measured results over both wide and narrow bandwidths.

II. MODE CHARTS, UNLOADED Q, AND SLOT COUPLING

The configurations of an SCDR loaded in a cylindrical and rectangular cavity is shown in Fig. 1(a) and (b), respectively. The SCDR consists of a conductor ring resonator of thickness t_c, inner radius r_1, and outer radius r_2. The conducting ring is sandwiched between two dielectric ring resonators of the same shape and size, each with thickness t_d, relative permittivity ε_r, and the spacing of the SCDR from the floor of the cavity is t. The dimensions of the enclosing cavity are radius r_3 and height c for the cylindrical cavity and a, b, and c for the rectangular cavity.

The dimensions, resonant frequency, and unloaded Q of two different SCDRs are presented in Table I. SCDR 2 is a much more compact element than SCDR 1, requiring only about 19% of the volume for a slightly lower resonant frequency. However, SCDR 1 is the element that will be used for filter design in the following section as a proof of concept of the SCDR element since the ceramics required were more readily available to the authors. Future research will focus on the more compact SCDR 2. The measured unloaded Q for SCDR 1 is 4700, which is slightly lower than the predicted value of 5892. For the SCDR prototype filter, the conducting resonator was made of copper, the cavity was made of aluminum, and the SCDR was supported by three radial Teflon posts. Silver plating both the conducting resonator and cavity would lead to a higher unloaded Q value. In order to analyze the lower order modes of the structure, the FDTD method for mode chart calculations presented in [25] has been used. To confirm the accuracy of the method, Table II compares measured results obtained for the SCDR in a cylindrical cavity of Fig. 1(a) with computed values obtained using FDTD and HFSS. The HFSS eigenmode solution used 3247 tetrahedra. As can be seen from Table II, the agreement between the measured data and those computed using the two different numerical methods is quite good. In particular, the results obtained using the FDTD method are very close to the measured values. The relative mode spectrum, as a function of the HE_{11}-mode resonant frequency, is also given in Table II, showing good separation of the higher order modes. Table III shows a comparison of the cavity volume, unloaded Q and Q_u/volume for a conductor loaded resonator, and the two types of SCDRs from Table I. The volume is divided by two because dual-mode resonators are used. Table III shows that SCDR 2 gives significantly higher Q_u/volume when compared with the conductor-loaded resonator.

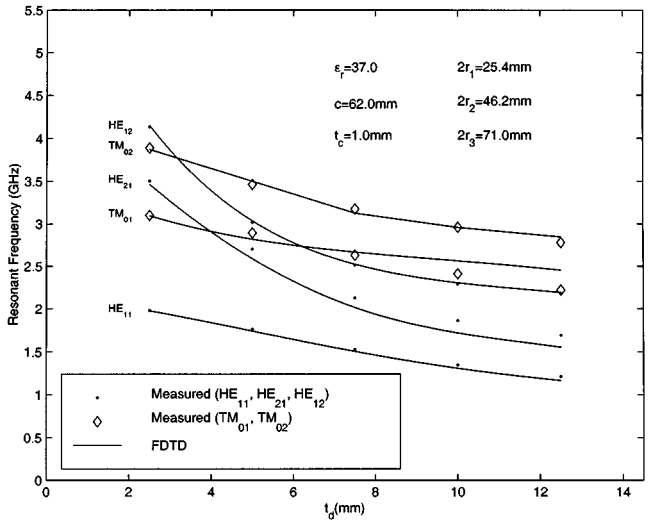

Fig. 2. Mode chart for an SCDR loaded in a cylindrical cavity versus the dielectric thickness t_d.

Fig. 2 depicts a mode chart that illustrates the effects on resonant frequency of increasing the dielectric thickness t_d of the SCDR. Both calculated and measured values are shown. The important thing to note from this figure is that *the mode separation has not been markedly effected by increasing the dielectric thickness of the resonator*. Hence, the resonator may be miniaturized without significantly degrading the spurious performance.

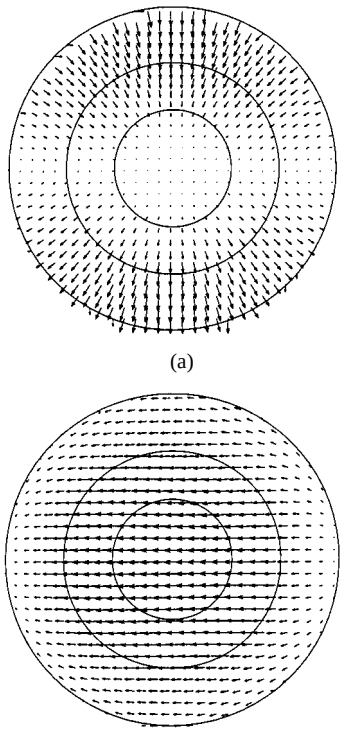

Fig. 3. SCDR tangential-field distribution plots for the HE_{11} mode at $z = 50$ mm. (a) Electric field. (b) Magnetic field.

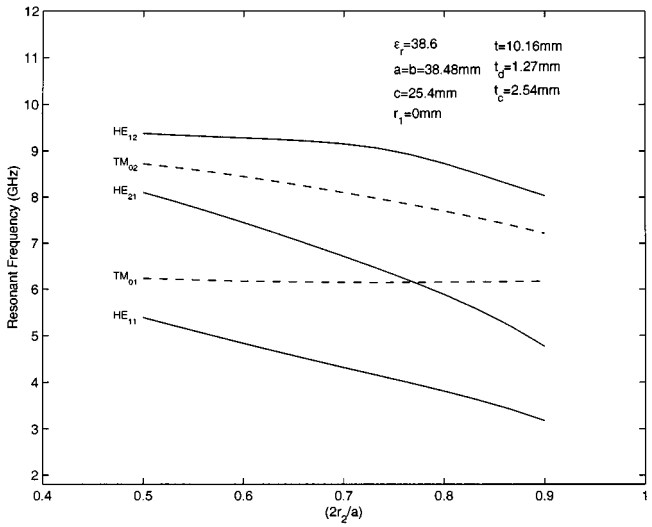

Fig. 4. Mode chart of resonant frequency versus the radius of the SCDR r_2.

Fig. 3 shows the electric- and magnetic-field distribution plots for the HE_{11}-mode SCDR calculated using the FDTD method. Comparison of these plots with those presented in [23] for the conductor-loaded resonator show the field patterns to be very similar. Fig. 4 shows the resonant frequencies versus the SCDR radius r_2 for an SCDR loaded in a rectangular cavity. This diagram shows the strong dependence on the radius of the SCDR for each mode, except the TM_{01} mode. In Fig. 5, the resonant frequency variation for an SCDR of a fixed size versus the height of the enclosing rectangular cavity is plotted. Fig. 6 shows the mode chart for resonant frequency versus the SCDR inner radius r_1, again for an SCDR loaded in a rectangular cavity. It is apparent from

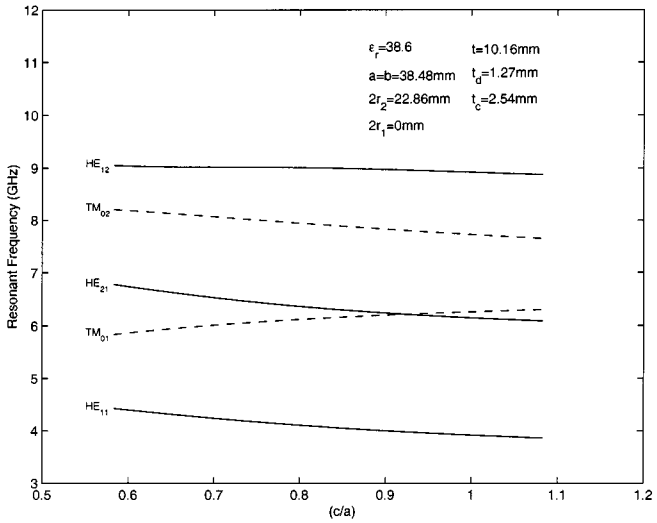

Fig. 5. Mode chart for a SCDR versus the height of the enclosing cavity c.

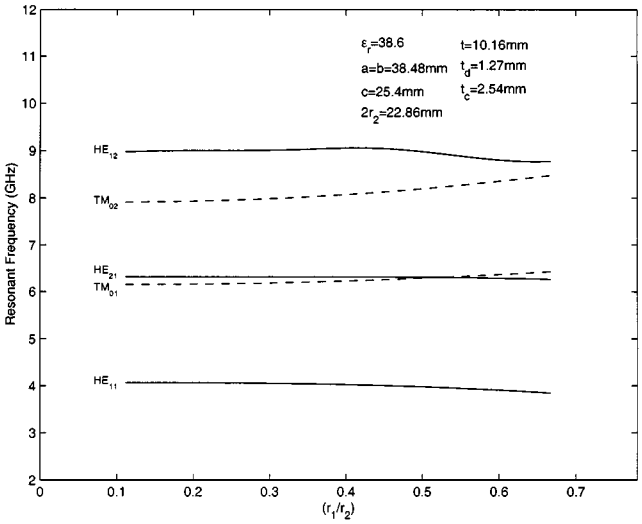

Fig. 6. Mode chart for a SCDR versus the inner radius r_1.

this diagram that there is a minimal effect on resonant frequency by introducing a concentric hole in the SCDR that can be used for placing a supporting dielectric structure of low permittivity in order to hold the resonator firmly in place.

Fig. 7 shows the variation in the conductor Q, dielectric Q, and unloaded Q as a function of the enclosing cavity radius, calculated using the technique described in [27]. It can be seen from this figure that the conductor Q dominates the unloaded Q for the SCDR. Slot-coupling coefficients for the HE_{11}-mode SCDR loaded in a cylindrical cavity have been calculated using the perfect electric conductor (PEC)/perfect magnetic conductor (PMC) wall technique and the FDTD method [27]. Measured and calculated results are presented in Fig. 8 and are quite close to one another. In order to couple orthogonally polarized HE_{11} SCDR modes, 45° coupling screws are needed. Screw coupling may be calculated using the technique of [28] and the following equation:

$$k = \frac{f_e^2 - f_m^2}{f_e^2 + f_m^2} \approx 2\,\frac{f_e - f_m}{f_e + f_m} \tag{1}$$

where f_e and f_m correspond to resonant frequencies when PEC and PMC walls are, respectively, placed at the structurally symmetric plane

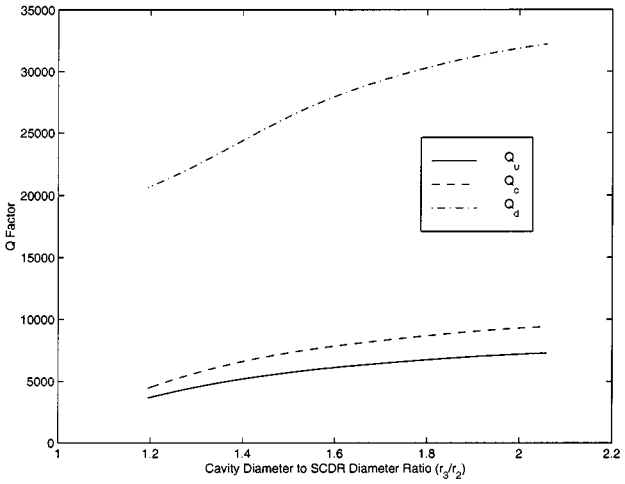

Fig. 7. Q_u, Q_c, and Q_d variation for the HE_{11}-mode SCDR dimensions of Table I as a function of cavity radius to SCDR radius. Cavity enclosure is copper with $\sigma_o = 5.80 \times 10^7$ S/m and $\overline{\sigma} = 0.9$ with $\tan\delta = 5.8 \times 10^{-5}$.

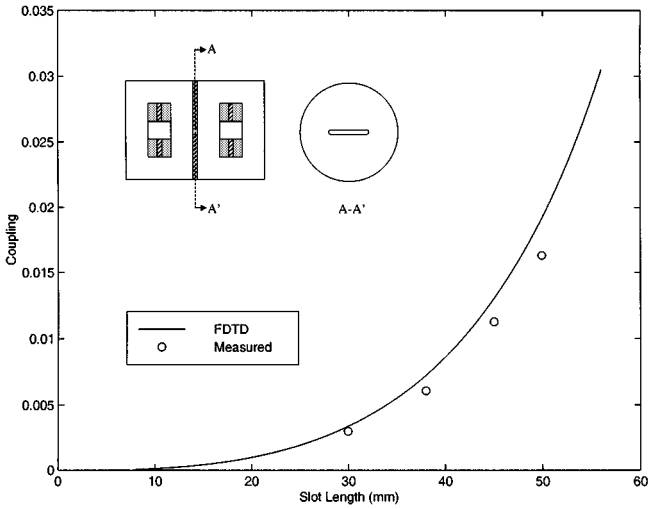

Fig. 8. Slot-coupling results for an SCDR with dimensions given in Table I. Slot width is 2.4 mm and slot thickness is 1.6 mm.

of the resonator. Screw coupling results calculated using the FDTD method are compared with measured values in Fig. 9.

Before building the four-pole filter, it is useful to examine the mode spectrum across the frequency band of interest for a one-pole SCDR filter. This takes into account the external coupling structures that will be used and their excitation of the various higher order modes. Fig. 10 shows the configuration of the one-pole SCDR filter. The measured wide-band mode spectrum, and that calculated using the FDTD method and the unmatched ports modal extraction technique [26] are shown in Figs. 11 and 12, respectively. The dimensions of the SCDR are given in Table I, and subminiature A (SMA) probes were used to realize the external coupling. The passband frequencies of the various modes correspond well between the measured and calculated results, however, there is some variation in the insertion-loss levels. As well as showing the SCDR-mode separation to be very good, the plots confirm that the TM_{01} mode is not excited by the external coupling structure.

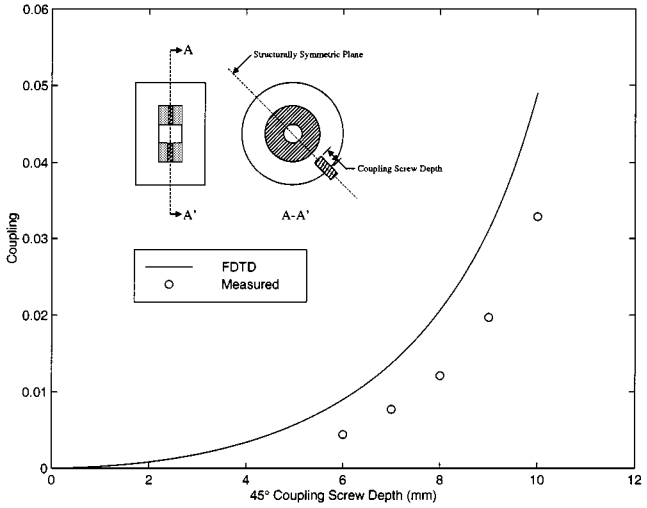

Fig. 9. Screw coupling results for an SCDR with dimensions given in Table I. Coupling screw diameter is 4 mm.

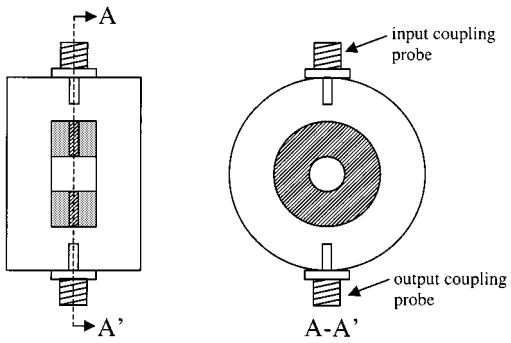

Fig. 10. Configuration of a one-pole SCDR filter used for mode spectrum analysis.

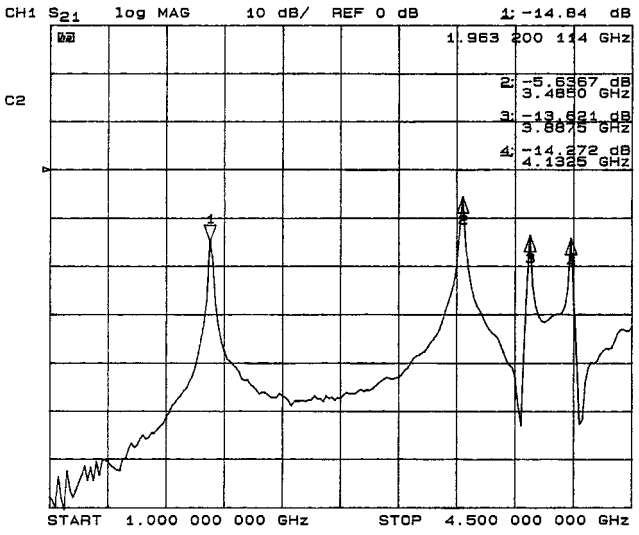

Fig. 11. Measured wide-band performance of a one-pole SCDR filter.

III. Four-Pole SCDR Filter

The configuration of the four-pole elliptic function SCDR filter is shown in Fig. 13. The filter center frequency is 1.910 GHz with a

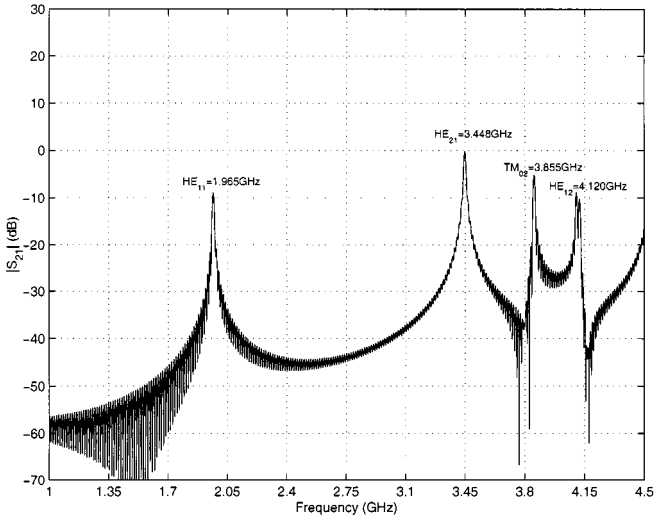

Fig. 12. Calculated wide-band performance of a one-pole SCDR filter.

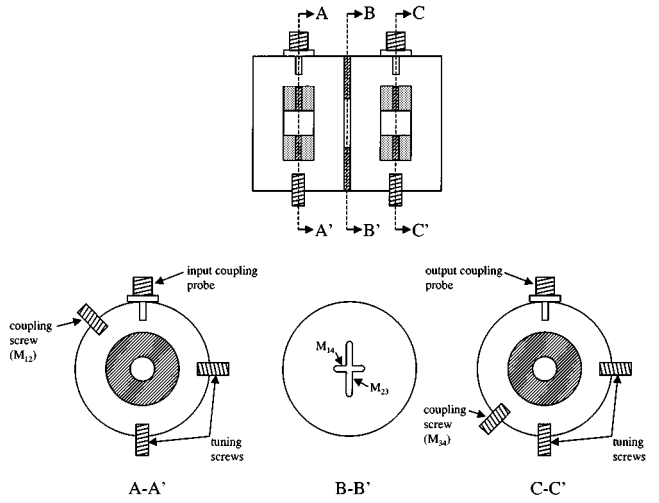

Fig. 13. Configuration of the elliptic function HE_{11}-mode four-pole SCDR filter.

16-MHz bandwidth. The normalized coupling matrix used for the filter design is

$$[m] = \begin{bmatrix} 0 & 0.980 & 0 & -0.110 \\ 0.980 & 0 & 0.788 & 0 \\ 0 & 0.788 & 0 & 0.980 \\ -0.110 & 0 & 0.980 & 0 \end{bmatrix}$$

$$R_1 = R_4 = 1.254. \tag{2}$$

The design frequency for the isolated SCDR was chosen as 1.977 GHz to take into account the loading effects of the coupling probes, coupling screws, and coupling posts. Coupling screws k_{12} and k_{34} were adjusted experimentally. Slot lengths for k_{23} and k_{14} were calculated from Fig. 8 to be 38.0 and 20.2 mm, respectively.

The theoretical response of the four-pole filter, calculated using the coupling matrix of (2), is shown in Fig. 14. The measured narrow-band performance of the SCDR filter is given in Fig. 15. Filter insertion loss at the center frequency was 0.77 dB, with a return loss of greater than 10 dB over the passband, and 22 dB at the center frequency. The realized unloaded Q of the filter was 3100 with the degradation caused by the insertion of tuning and coupling screws and the brass cross-slotted coupling plate between the two cavities.

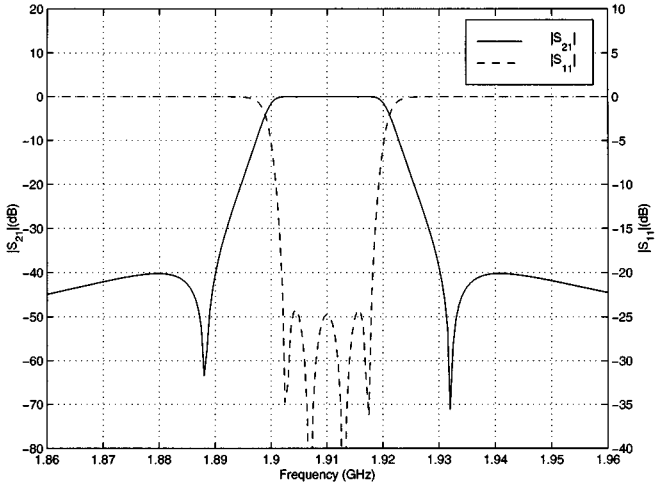

Fig. 14. Theoretical response of the SCDR four-pole elliptic function filter.

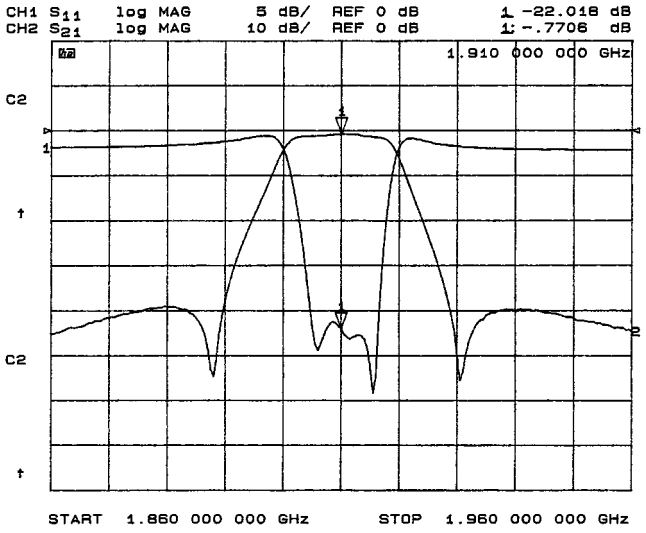

Fig. 15. Measured narrow-band performance of the four-pole SCDR elliptic function filter.

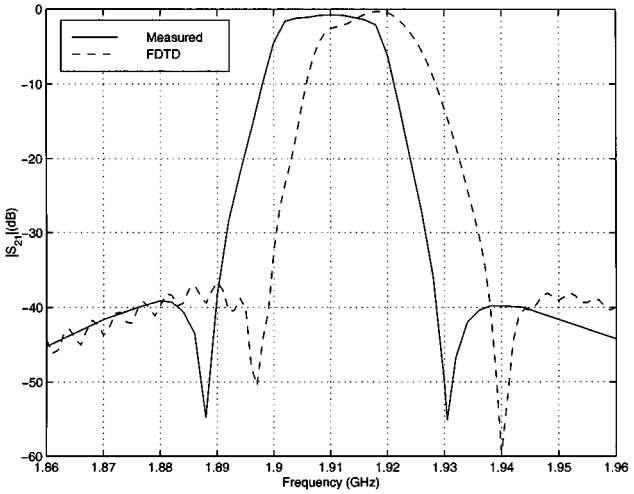

Fig. 16. Calculated and measured narrow-band performance of the four-pole SCDR elliptic function filter.

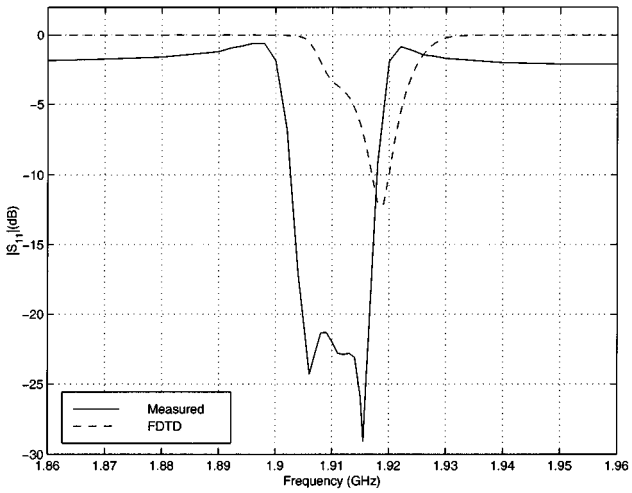

Fig. 17. Calculated and measured narrow-band performance of the four-pole SCDR elliptic function filter.

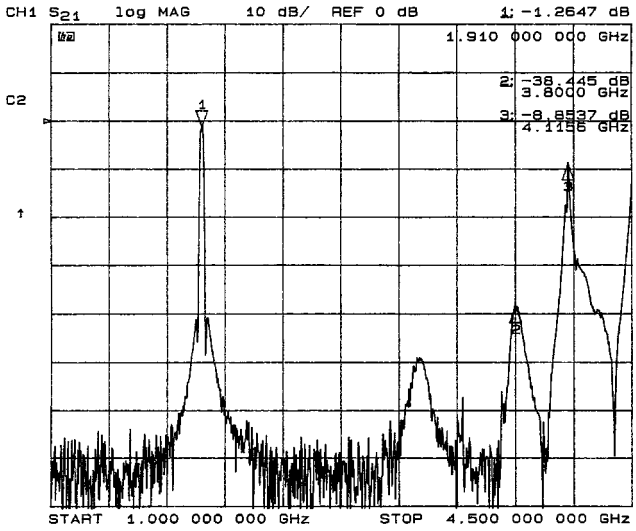

Fig. 18. Measured wide-band spurious performance of the four-pole SCDR elliptic-function filter.

Narrow- and wide-band S-parameters have been computed for the four-pole HE_{11} SCDR filter using the FDTD method, Mur's absorbing boundary condition (ABC), and unmatched port modal S-parameter extraction [26], [27]. The FDTD mesh size was 143 $\times$ 252 $\times$ 209, discretization of 0.5 mm, and 240 000 time steps were required. The FDTD code was run on a 128-node CM5 computer and required 691 MB of memory and 16.0 h of CPU time to compute. Narrow-band insertion-loss and return-loss diagrams computed using the FDTD method are compared with measured results in Figs. 16 and 17, respectively. The computed $|S_{21}|$ value shows good agreement in the relative positions of the transmission zeros, the slope of the filter skirt outside the passband, and the level of the elliptic function sidelobes. However, the passband flatness is not correctly predicted, leading to a significant discrepancy in the calculated $|S_{11}|$ value. The main reasons for the discrepancies could be attributed to the inherent dispersion in the FDTD algorithm and the truncation of the time series used in the calculations before the fields have stopped oscillating completely.

The measured wide-band spurious performance of the SCDR filter is shown in Fig. 18. The spurious suppression is greater than 38 dB from the center frequency up to 4.054 GHz, or 2.12 f_0, which is a large improvement over conventional dual-mode DR filters. Both the HE_{21} and TM_{01}-mode passbands have been suppressed, with the dominant spurious passband resulting from the HE_{12} mode. The wide-band spurious performance calculated using the FDTD method is given in Fig. 19. The locations of the spurious passbands have been accurately predicted; however, their levels, particularly the HE_{21} mode, are not as accurate. Overall, for such a complicated structure, the FDTD simulations compare well with measured results, and provide valuable insights into the SCDR filter performance. Using the design information, the filter was readily constructed and tuned, and its prescribed performance was met using the calculated dimensions.

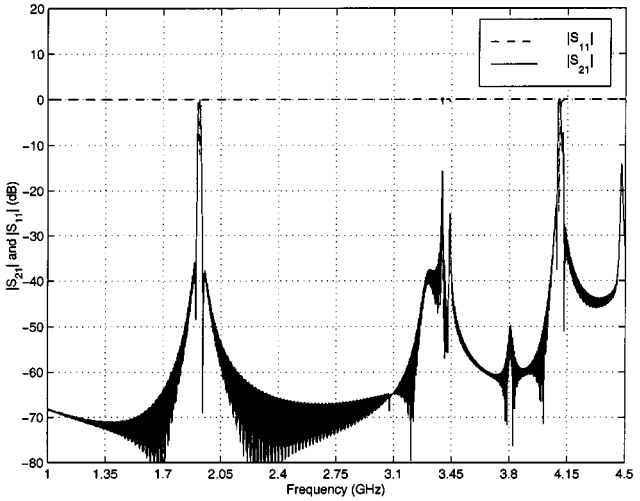

Fig. 19. Wide-band spurious performance of the four-pole SCDR elliptic filter calculated using the FDTD method.

IV. Conclusions

Filters based on a new resonant element, i.e., the SCDR, have been introduced and their performance evaluated through FDTD simulation and measurement. It is shown that the merits of the SCDR lies in improved spurious rejection, and high unloaded Q per volume when compact configurations are used. The added advantage of the SCDR configuration is that spurious performance does not degrade with reduction in size (see Fig. 2), thus lending itself well to miniaturization. Resonant frequencies for the lower order modes were accurately predicted. Mode charts, slot coupling, screw coupling, and unloaded Q graphs were also presented. S-parameters were calculated for one- and four-pole SCDR filters and compared with measured values. The four-pole filter measured spurious suppression was greater than 38 dB from the center frequency of 1.910 GHz up to 4.054 GHz, or 2.12 f_0 with a passband insertion loss of 0.77 dB. Narrow- and wide-band S-parameters calculated for the four-pole filter using the FDTD method gave close agreement with measured results. Issues related to the use of SCDR filters for high-power applications will be investigated in the future.

Acknowledgment

The authors would like to thank the New South Wales Centre for Parallel Computing (NSWCPC), N.S.W., Australia, for providing access to CM5 computing facilities.

References

[1] Y. Kobayashi and M. Miura, "Optimum design of shielded dielectric rod and ring resonators for obtaining the best mode separation," in *IEEE MTT-S Int. Microwave Symp. Dig.*, 1984, pp. 184–186.

[2] S.-W. Chen and K . A. Zaki, "Dielectric ring resonators loaded in waveguide and on substrate," *IEEE Trans. Microwave Theory Tech.*, vol. 39, pp. 2069–2076, Dec. 1991.
[3] K. Wakino, T. Nishikawa, H. Matsumoto, and Y. Ishikawa, "Quarter wave dielectric transmission line diplexer for land mobile communications," in *IEEE MTT-S Int. Microwave Symp. Dig.*, 1979, pp. 278–280.
[4] C. L. Ren, "Mode suppressor for dielectric resonator filters," in *IEEE MTT-S Int. Microwave Symp. Dig.*, 1982, pp. 389–391.
[5] R. V. Snyder, "Dielectric resonator filters with wide stopbands," *IEEE Trans. Microwave Theory Tech.*, vol. 40, pp. 2100–2103, Nov. 1992.
[6] V. Madrangeas, M. Aubourg, P. Guillon, S. Vigneron, and B. Theron, "Analysis and realization of L-band dielectric resonator microwave filters," *IEEE Trans. Microwave Theory Tech.*, vol. 40, pp. 120–127, Jan. 1992.
[7] Y. Kobayashi and M. Minegishi, "A low-loss bandpass filter using electrically coupled high-Q $\mathrm{TM}_{01\delta}$ dielectric rod resonators," *IEEE Trans. Microwave Theory Tech.*, vol. 36, pp. 1727–1732, Dec. 1988.
[8] T. Nishikawa, K. Wakino, K. Tsunoda, and Y. Ishikawa, "Dielectric high-power bandpass filter using quarter-cut $\mathrm{TE}_{01\delta}$ image resonator for cellular base stations," *IEEE Trans. Microwave Theory Tech.*, vol. MTT-35, pp. 1150–1155, Dec. 1987.
[9] H. J. Riblet, "Waveguide filter having nonidentical sections resonant at same fundamental and different harmonic frequencies," U.S. Patent 3 153 208, 1964.
[10] K. Wakino, T. Nishikawa, H. Matsumoto, and Y. Ishikawa, "Miniaturized band pass filters using half wave dielectric resonators with improved spurious response," in *IEEE MTT-S Int. Microwave Symp. Dig.*, 1978, pp. 230–232.
[11] Y. Kobayashi and C. Inoue, "Bandpass and bandstop filters using dominant $\mathrm{TM}_{01\delta}$ mode dielectric rod resonators," in *IEEE MTT-S Int. Microwave Symp. Dig.*, 1997, pp. 793–796.
[12] R. R. Bonetti and A. E. Williams, "A narrowband filter with a wide spurious-free stopband," in *IEEE MTT-S Int. Microwave Symp. Dig.*, 1992, pp. 1331–1333.
[13] J.-F. Liang, K. A. Zaki, and A. E. Atia, "Mixed modes dielectric resonators filters," *IEEE Trans. Microwave Theory Tech.*, vol. 42, pp. 2449–2454, Dec. 1994.
[14] C. Wang, H.-W. Yao, K. A. Zaki, and R. R. Mansour, "Mixed modes cylindrical dielectric resonator filters with rectangular enclosure," *IEEE Trans. Microwave Theory Tech.*, vol. 43, pp. 2817–2823, Dec. 1995.
[15] H. Y. Hwang, N. S. Park, H. Y. Cho, S. W. Yun, and I. S. Chang, "The design of bandpass filters made of both dielectric and coaxial resonators," in *IEEE MTT-S Int. Microwave Symp. Dig.*, 1997, pp. 805–808.
[16] J.-F. Liang and W. D. Blair, "High-Q TE_{01} mode DR filters for PCS wireless base stations," *IEEE Trans. Microwave Theory Tech.*, vol. 46, pp. 2493–2500, Dec. 1998.
[17] C. Wang, K. A. Zaki, and A. E. Atia, "Dual-mode combined dielectric and conductor loaded cavity filters," in *IEEE MTT-S Int. Microwave Symp. Dig.*, 1997, pp. 1103–1106.
[18] A. Abdelmonem, J.-F. Liang, H.-W. Yao, and K. A. Zaki, "Full wave design of spurious free DR TE mode bandpass filter," *IEEE Trans. Microwave Theory Tech.*, vol. 43, pp. 744–752, Apr. 1995.
[19] R. V. Snyder and C. Alvarez, "Filters using a new type of resonator: The partially-metallized dielectric slug," in *IEEE MTT-S Int. Microwave Symp. Dig.*, 1999, pp. 1029–1032.
[20] I. C. Hunter, J. D. Rhodes, and V. Dassonville, "Dual-mode filters with conductor loaded dielectric resonators," *IEEE Trans. Microwave Theory Tech.*, vol. 47, pp. 2304–2311, Dec. 1999.
[21] H.-W. Yao, K. A. Zaki, A. E. Atia, and T. G. Dolan, "Improvement of spurious performance of combline filters," in *IEEE MTT-S Int. Microwave Symp. Dig.*, 1997, pp. 1099–1102.
[22] C. Wang, K. A. Zaki, A. E. Atia, and T. G. Dolan, "Dielectric combline resonators and filters," *IEEE Trans. Microwave Theory Tech.*, vol. 46, pp. 2501–2506, Dec. 1998.
[23] C. Wang and K. A. Zaki, "Conductor loaded resonator filters with wide spurious-free stopbands," *IEEE Trans. Microwave Theory Tech.*, vol. 45, pp. 2387–2392, Dec. 1997.
[24] A. R. Weily and A. S. Mohan, "Sandwiched conductor dielectric resonator filters for wideband spurious-free performance," in *Proc. Asia–Pacific Microwave Conf.*, 1998, pp. 1359–1362.
[25] ——, "Mode-chart calculation for dielectric- and conductor-loaded resonators using modal extraction and FDTD," *Microwave Opt. Technol. Lett.*, vol. 21, no. 6, pp. 405–411, June 1999.
[26] ——, "Full two-port analysis of coaxial probe fed TE_{01} and HE_{11} mode dielectric resonator filters using FDTD," *Microwave Opt. Technol. Lett.*, vol. 18, no. 2, pp. 149–154, June 1998.
[27] ——, "Design and wideband spurious performance prediction for a mixed resonator combline/TE_{01}-mode DR filter using FDTD," *Microwave Opt. Technol. Lett.*, vol. 23, no. 5, pp. 266–273, Dec. 1999.
[28] X.-P. Liang, K. A. Zaki, and A. E. Atia, "Dual mode coupling by square corner cut in resonators and filters," *IEEE Trans. Microwave Theory Tech.*, vol. 40, pp. 2294–2302, Dec. 1992.

Microwave Transformers, Inductors, and Transmission Lines Implemented in an Si/SiGe HBT Process

David C. Laney, Lawrence E. Larson, Paul Chan, John Malinowski, David Harame, Seshu Subbanna, Rich Volant, and Michael Case

***Abstract*—Experimental results are presented on microwave inductors, transformers, and transmission lines fabricated in an Si/SiGe heterojunction-bipolar-transistor process with standard metallization and a thick polyimide dielectric. Microstrip transmission lines with characteristic impedances from 44 to 73 Ω, Q's from 10 to 14, and insertion losses from 0.11 to 0.16 dB/mm at 10 GHz are presented. Conventional planar inductors with inductances from 0.5 to 15 nH and with peak Q's up to 22 are presented. Lateral transformers with a maximum available gain of better than -5 dB and a measured coupling coefficient (k) of 0.6 at 5.5 GHz and 0.4 up to 12.5 GHz are also discussed.**

***Index Terms*—Inductors, integrated circuit fabrication, MMICs, transformers, transmission lines.**

I. Introduction

In this paper, we present the performance of microstrip transmission lines, standard square planar inductors, and bilayer planar transformers produced with standard silicon very large scale integration (VLSI) Al–Cu metallization and a thick polyimide dielectric. In this process, the top metal (TM) layer is the standard back-end metallization, and the metal layer above the top layer, the last metal (LM) layer, is separated from the TM layer by 12 μm of polyimide (Fig. 1).

II. Silicon-Based Transmission-Line, Inductor, and Transformer Design

The design of microstrip structures, inductors, and transformers is well known in planar microwave-circuit technology. References [1]–[5], [7], and [9]–[12] provide important background.

Manuscript received April 27, 1999; revised September 22, 2000.

D. C. Laney is with the Department of Electrical and Computer Engineering, University of California at San Diego, La Jolla, CA 92093 USA and also with HRL Laboratories LLC, Malibu, CA 90265 USA.

L. E. Larson is with the Department of Electrical and Computer Engineering, University of California at San Diego, La Jolla, CA 92093 USA.

P. Chan was with Hughes Space and Communications, El Segundo, CA 90245 USA. He is now with Qualcomm Inc., San Diego, CA 92121 USA.

J. Malinowshi and D. Harame are with IBM Microelectronics, Essex Junction, VT 05452 USA.

S. Subbanna and R. Volant are with IBM Microelectronics, Hopewell Junction, NY 12533 USA.

M. Case was with HRL Laboratories LLC, Malibu, CA 90265 USA. He is now with the IBM Corporation, Encinitas, CA 92024 USA.

Publisher Item Identifier S 0018-9480(01)06142-7.